Technion - Israel Institute of Technology

Advanced Applications in Inertial Navigation Systems (018827)

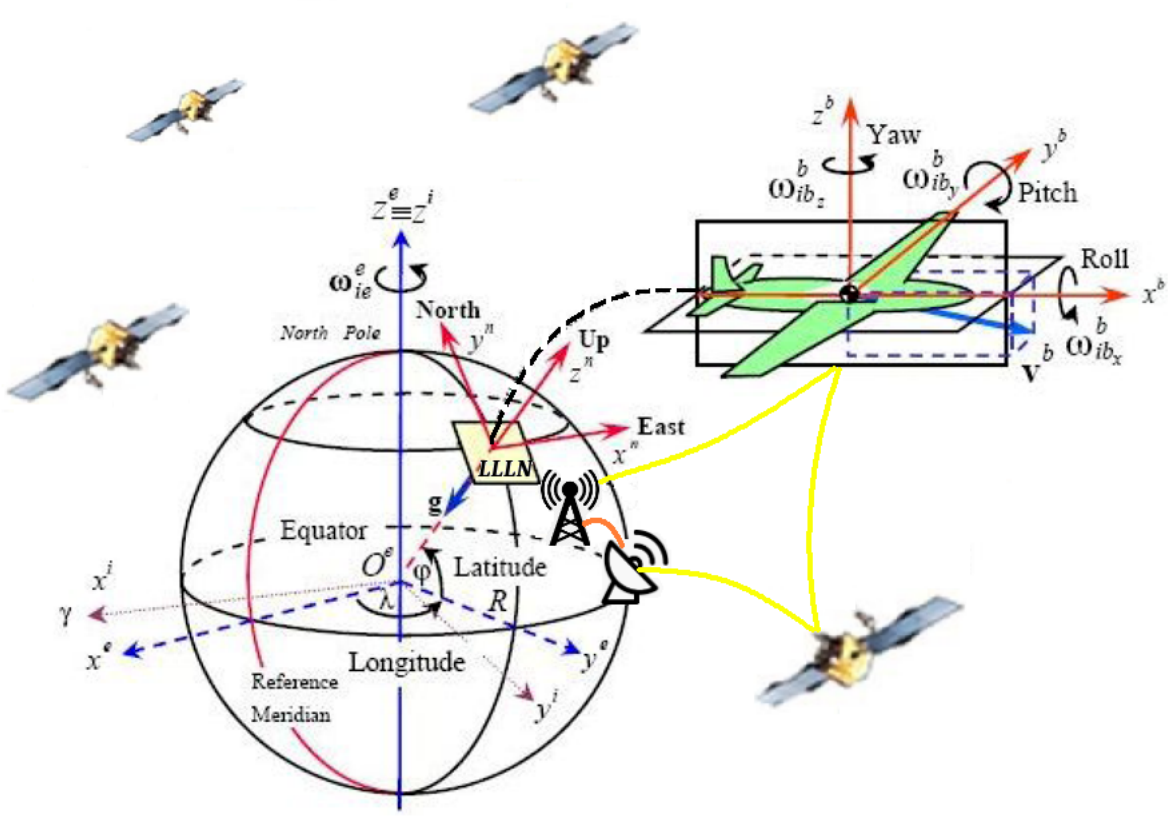

Omri Asraf ⊕ Daniel Engelsman @ September 3, 2019

= Final Report =

Contents

1 Abstract

In this report we show several tasks that we have been working along :

(i) Implementing the strapdown model learnt in class, utilizing IMU inputs.

(ii) Implementing the error state model learn in class, and integrate it with the strapdown.

(iii) Implementing an Extended Kalman Filter with respect to the mentioned above

(iv) Observability analysis of the model, based on our chosen paper :

"Monitoring Degree of Observability in GPS/INS Integration".

The paper implements the concept of 'Degree of Observability' (=**DoO**) with respect to GPS/INS integrated systems, and is discussed either theoretically and experimentally. The traditional observability analysis is inadequate for an extraordinary navigation scenarios as the $\mathcal{O}$ matrix becomes very large for high order time variant system, such that it rises computational difficulties. The paper aims to introduce a practical approach for the observability measuring, which is bounded by the system's n relevant states.

2 Introduction

As mentioned above, the paper focuses on an observability analysis of a GPS/INS integration, using a Kalman Filter (=**KF**). The main motivation for observability analysis in a dynamic system, is its capability to determine the KF efficiency upon the estimated states, with respect to (=**w.r.t**) the noise and measurement noise.

However, an un-observable system would not yield an accurate estimation [1] and is prone to divergence [2], even if the noise level is negligible. Thus, the observability imposes a lower bound for the estimation error.

In our project we simulate the DoO evolution along the integration process w.r.t to the error covariance matrix of the current time step (section **3.3**). Further literature review is detailed comprehensively at the References section **5**.

3 Problem formulation

Similar but different to the paper's model, our model sticks to the course' textbooks [3]. That is to say that we are dealing with two state spaces : Navigation states and Error states. Only the latter is being estimated, and thus been developed.

3.1 Error state model

Let the first order state space, governed by the following dynamics :

$$\dot{x}(t) = f(x(t), t) + w \qquad \Leftrightarrow \qquad \dot{x} = Fx + Gu + w \tag{3.1}$$

$$z(t) = h(x(t), t) + v \qquad \Leftrightarrow \qquad z = Hx + v \tag{3.2}$$

$F_k = \frac{\partial f}{\partial x}\Big|_{\hat{x_k}, u_k}$ - dynamic matrix

$H = \frac{\partial h}{\partial x}\Big|_{\hat{x_k}}$ - observation matrix

G - noise distribution matrix

w - process noise vector

x - state estimate vector

v - measurement noise vector

The matrices' contents are fully developed in one of the course textbook [4], such that our error model utilizes nine states, each has a 3D navigation solution [5] :

$$\bar{x} \;=\; \delta x \;=\; [\delta p^n \quad \delta v^n \quad \delta \varepsilon^n]^T \tag{3.3}$$

The corresponding discrete-time linear system will be expressed as follows :

$$x_k = \Phi_{k-1} x_{k-1} + G_{k-1} w_{k-1} \;, \quad w_{k-1} \sim N(0,\; Q_k) \tag{3.4}$$

$$z_k = H_k x_k + v_k \qquad\qquad , \quad v_{k-1} \sim N(0,\; R_k) \tag{3.5}$$

Φ_k - transition matrix [6]

w, v - zero mean white noise

The transition and observation matrices' dimensions are :

$$\Phi \;\in\; \mathbb{R}^{9\times 9} \qquad\qquad H = [I_{3\times 3} \quad 0_{3\times 6}]$$

3.2 Extended Kalman Filtering

In a perfect world where measurements are perfectly describing the environment's physics, no complex error model is needed. However the stochastic nature of a noisy measurement tends to drift when integrated over time, as seen in the following ω_x example [10] :

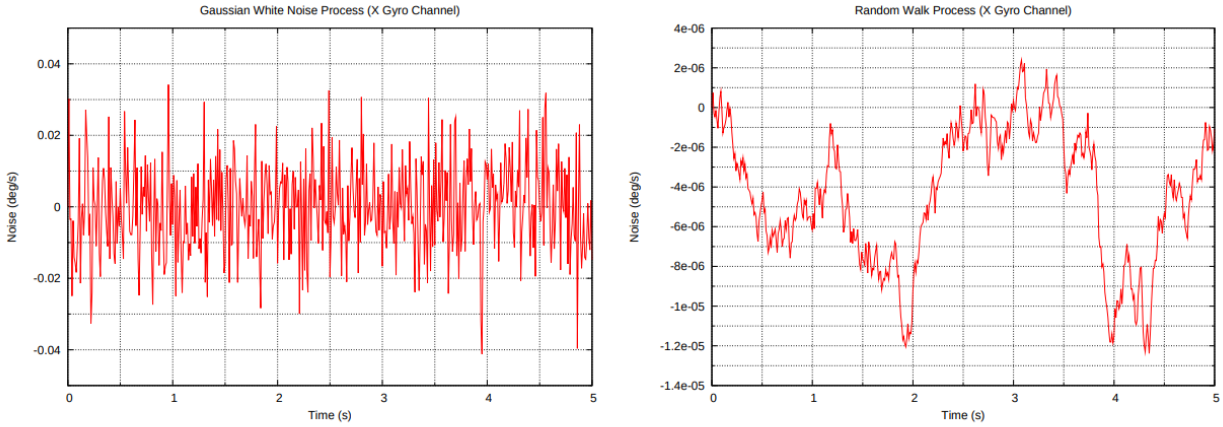

(a) White noise sequence

(b) Random walk sequence

This behavior collide with our intention to get good navigation results as it quickly looses track with reality. It is therefore necessary to estimate the error state w.r.t the navigation state, and this can be done using the Kalman Filtering (=**KF**) :

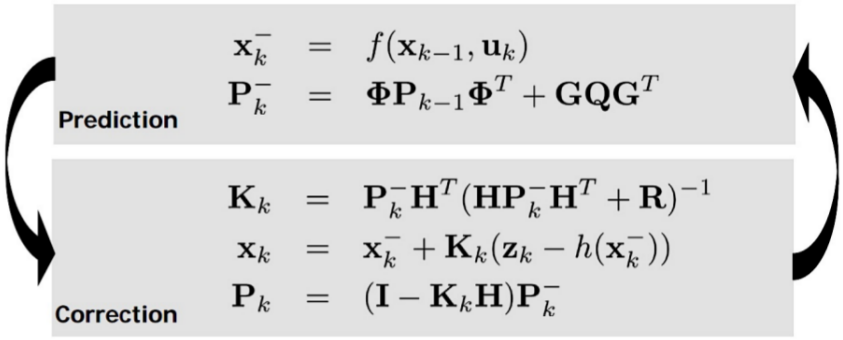

Figure 1: Kalman Filter flowchart

The prediction is the default phase of the model, that is promoted iteratively by each IMU measurement, and thus drifts away from real trajectory. The state's correction, occurs whenever an external GPS position measurement is available. Here :

$$\text{fusion ratio} \ : \quad \frac{f_{GPS}}{f_{IMU}} = \frac{1\ [Hz]}{100\ [Hz]} \ = \ 1:100 \tag{3.6}$$

The correction puts the user back on track as it truncates the navigation error and attenuates the evolving drift over time. Following is a flow diagram of our model :

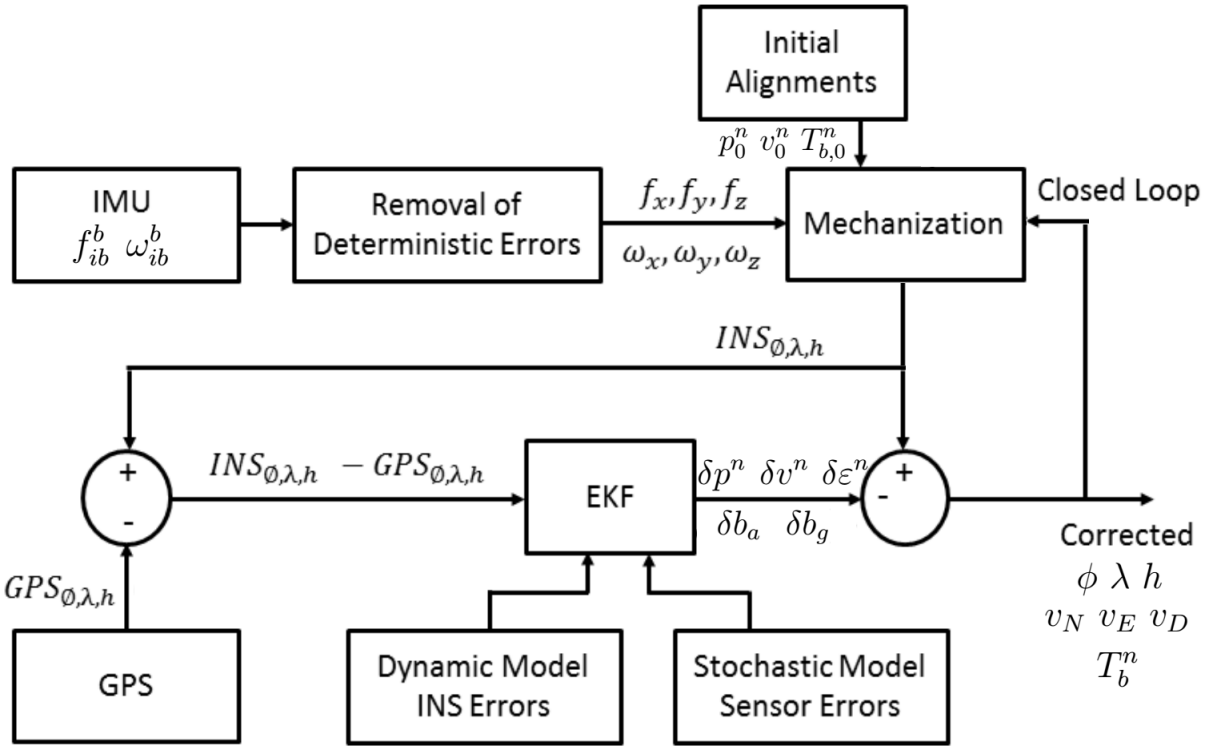

Figure 2: Closed loop loosely coupled integration

As seen, the EKF block is responsible for updating the error state. Most of the time performing prediction w.r.t IMU measurements, and applying correction once an external GPS is available. The loop closes finally as the navigation state is being updated, and then propagating back the next prediction.

3.3 Observability analysis

"Observability is a measure of how well internal states of a system can be inferred from knowledge of its external outputs" [8]. Here, in our non-linear system, $H(t) = I_{3\times3}$ is time constants, thus we check observability by the boolean condition : $\text{rank}(\mathcal{O}_v) \stackrel{?}{=} \text{rank}(\mathcal{O}_{v+1})$.

$$Let \quad \mathcal{O} = \begin{bmatrix} N_0(t) \\ N_1(t) \\ \vdots \\ N_{v-1}(t) \end{bmatrix} \Rightarrow \begin{bmatrix} H_0(t) \\ H_0(t)F(t) + \cancelto{0}{\frac{\partial}{\partial t}H_0(t)} \\ \vdots \\ H_{v-1}(t)F(t) + \cancelto{0}{\frac{\partial}{\partial t}H_{v-1}(t)} \end{bmatrix} \Rightarrow \begin{bmatrix} H \\ HF \\ \cdots \\ HF^{v-1} \end{bmatrix} \tag{3.7}$$

However, here the author utilizes the 'degree of observability' analysis, which is a quantitative approach devised firstly by Ham et al. (1983) [9]. During the KF cycle, we obtain an error covariance (=P) that reflects the error between real and estimated states, such that observability information can be derived through a proper mathematical analysis of P. Conveniently we'll present the normalized error (P'):

$$P'(k) = \Big(\sqrt{P(0)}\Big)^{-1} P(k) \Big(\sqrt{P(0)}\Big)^{-1} \tag{3.8}$$

$\circ$ $P(0)$ = initial error covariance matrix $\quad$ $\circ$ $P(k)$ = current error covariance matrix

The obtained matrix can be written in a matrix presentation as follows :

$$P'(k) = \begin{bmatrix} \frac{P_{11}}{P_{11}(0)} & \frac{P_{12}}{\sqrt{P_{11}(0)P_{22}(0)}} & \cdots & \frac{P_{12}}{\sqrt{P_{11}(0)P_{nn}(0)}} \\ \frac{P_{21}}{\sqrt{P_{22}(0)P_{11}(0)}} & \frac{P_{11}}{P_{22}(0)} & \cdots & \frac{P_{12}}{\sqrt{P_{22}(0)P_{nn}(0)}} \\ \vdots & \vdots & \ddots & \vdots \\ \frac{P_{n1}}{\sqrt{P_{nn}(0)P_{11}(0)}} & \frac{P_{n2}}{\sqrt{P_{nn}(0)P_{22}(0)}} & \cdots & \frac{P_{nn}}{\sqrt{P_{nn}(0)}} \end{bmatrix} \tag{3.9}$$

P_{ij} and $P_{ij}(0)$ are the original error covariance matrix elements, $P(k)$ and $P(0)$ respectively. The sum of all of the eigenvalues of a matrix equals to the trace, such that after few manipulations we get the normalized error covariance :

$$P''(k) = \frac{n}{\text{tr}\Big(P'(k)\Big)} P'(k) \tag{3.10}$$

The eigenvalues of $P''(k)$ are dimensionless and bounded between $0 < \lambda_i \leq n$, such that the DoO is defined better, as the error turns smaller.

4 Simulation

In this section we will show our implementation for the INS/GPS model. The data is presented either in standard graphs and video links to some real-time presentations.

4.1 Scenario properties

A confident model level has to be well validate before diving into complex scenarios. Thus, we have carefully chose a convenient case where the following kinematics is perfromed :

$$f_{ib}^{b} = \begin{bmatrix} 0 \\ 0.087 \\ g \end{bmatrix} [\frac{m}{sec^2}] \qquad \omega_{ib}^{b} = \begin{bmatrix} 0 \\ 0 \\ \pi/30 \end{bmatrix} + \begin{bmatrix} \omega_{ie}\cos(\phi) \\ 0 \\ -\omega_{ie}\sin(\phi) \end{bmatrix} [\frac{rad}{sec}] \qquad \begin{bmatrix} t \\ R \\ \Sigma l \end{bmatrix} \sim \begin{pmatrix} 61[sec] \\ 8[m] \\ 50[m] \end{pmatrix}$$

Such that we start from the origin at t_0 and moving in a constant angular velocity ω_z :

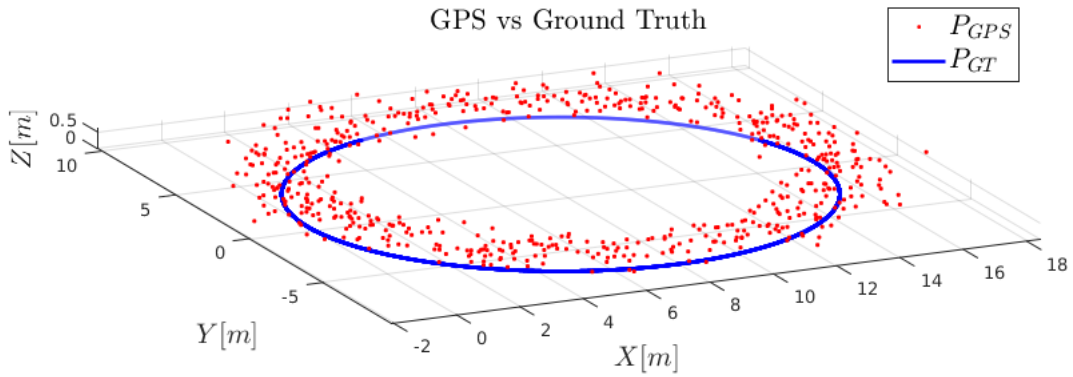

Figure 3: The scenario demonstration

In order to simulate the stochastic nature of errors, one has to deliberately "corrupt" the measurements with a deterministic error ($\sigma \in \mathbb{R}^{3\times3}$) :

$$\sigma_{acc} = 500\ [\mu g] \quad \sigma_{\omega} = 10^{-9}\ [\frac{rad}{sec}] \quad \Rightarrow \quad Q_k = \Sigma_{Proc.} = diag(\ [\ \sigma_{acc}^T\ \ \sigma_{\omega}^T\ \ 0_{3\times1}]^2\ ) \ \in \ \mathbb{R}^{9\times9}$$

$$\sigma_{GPS} \sim 1\ [m] \quad \Rightarrow \quad R_k = \Sigma_{Meas.} = diag(\qquad [\ \sigma_{GPS}^T]^2 \qquad) \ \in \ \mathbb{R}^{3\times3}$$

Following is the scenario's noisy IMU measurements :

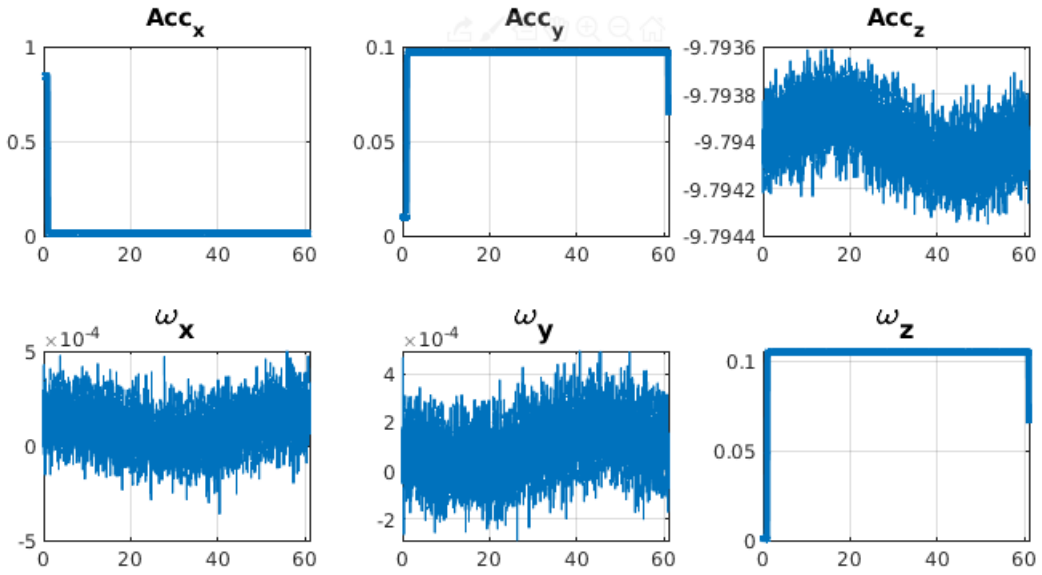

Figure 4: IMU measurements along run

Note that all axes are noisy, but the scenario is dictated mainly by f_y^b and ω_z inputs.

4.2 Online Demonstrations

Attached with the file are two *YouTube* links to an online simulation :

(i) EKF estimation performance w.r.t several IMU/GPS fusion ratio, and thus the evolving of each corresponding error.

(ii) EKF estimation of full execution under 1:100 IMU/GPS fusion ratio.

These footage show the position states of both navigation and error, and demonstrate the influence of the fusion ratio, formulated at Eq. **3.6**.

4.3 Error state results

Let's examine the estimation performance over time, starting with the position error :

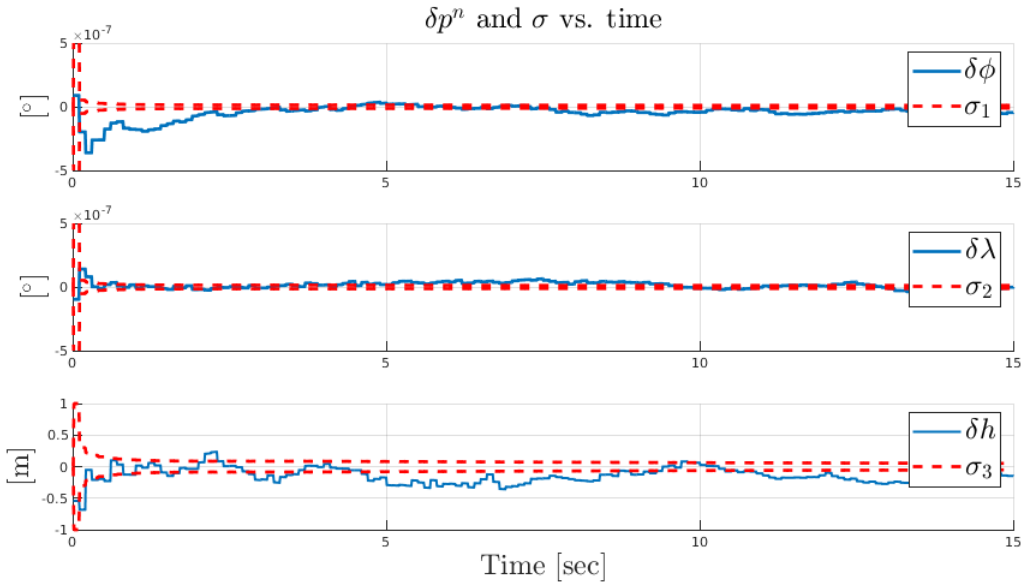

Both subplots exhibit decay from initial value along time, and the *red* dashed line stands for the corresponding standard deviation. We can see that the geodetic angle errors (ϕ, λ) exhibit slight changes that approache zero, since the model moves only few meters in the LLLN frame. Contrarily, the altitude is scaled in meters w.r.t previous samples, such that the error magnitude is much bigger. Now let's check the velocity error states :

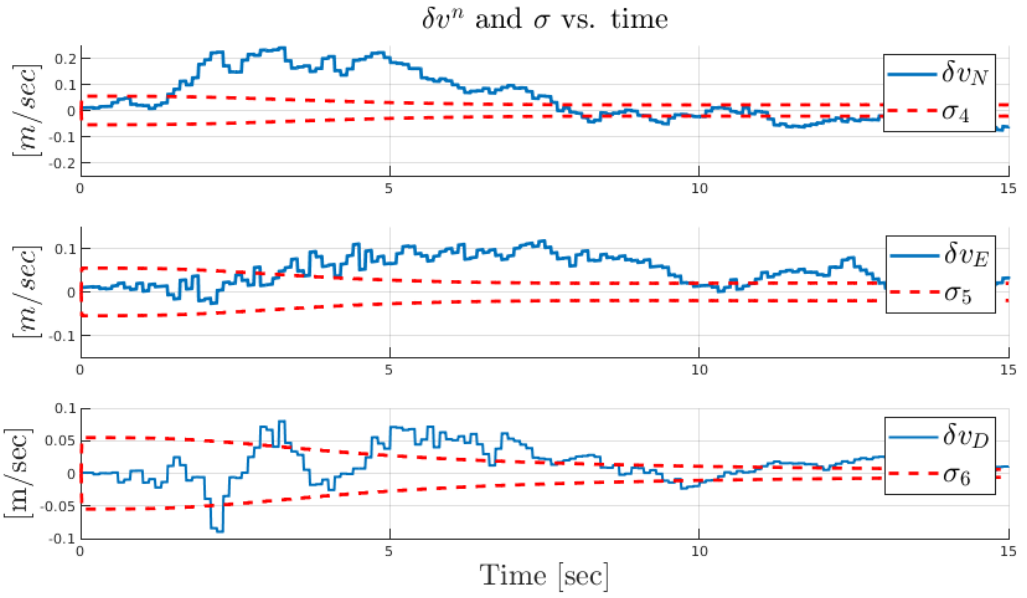

Unlike the position that is being corrected by the observation itself ($\tilde{z}_{GPS}$), here the errors worsen along time, as they evolve in a *random walk*. v_N and v_E show noisy behavior while v_D manages to stabilize after a while, as it can be explained by our strapdown model's inaccuracies. Next is the Euler angles error extracted from the orientation states - T_b^n :

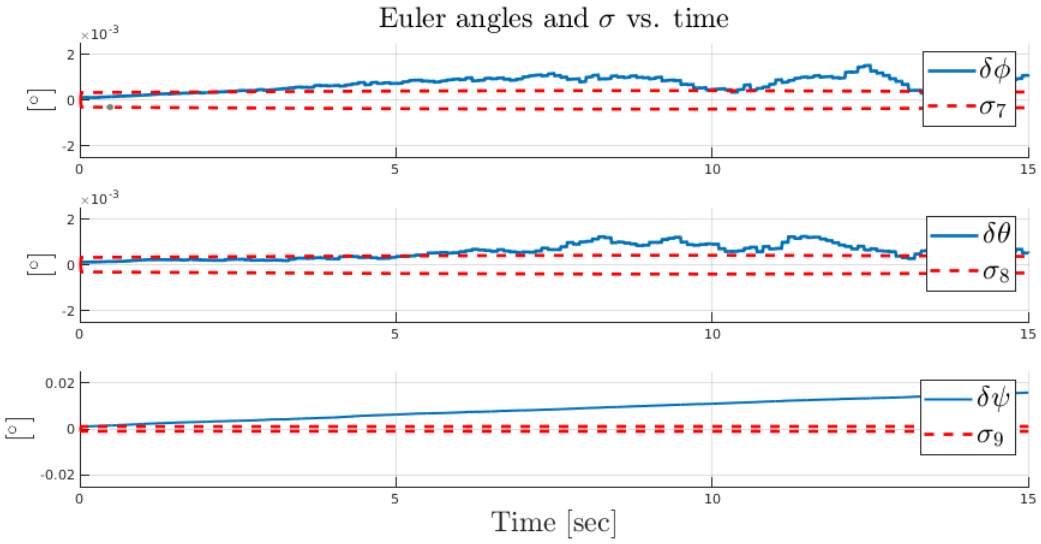

On the left axis (ϕ - roll, θ - pitch) we can see only minor changes exerting on the model, which makes sense for its planar movement. Contrarily, the azimuthal ($\delta\psi$) change is dramatically bigger as it's the main action axis in the motion's orientation.

4.4 Degree of Observability results

We'll now show the DoO analysis based on section **3.3**, and see if we can determine which states are being best estimated (↓ DoO), and which are most weakly (↑ DoO).

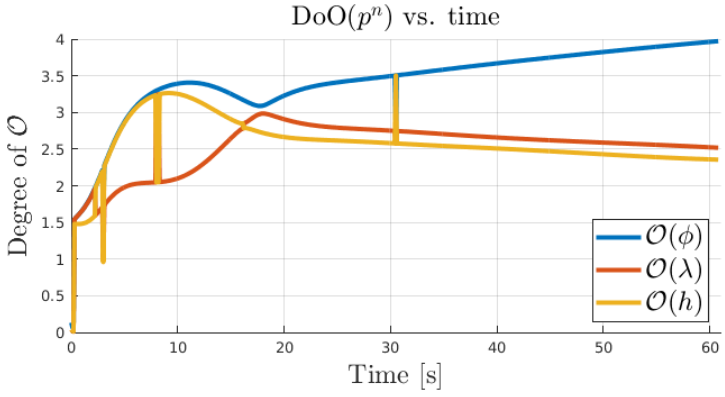

The geodetic degrees initially perform a hunchback raise, but then slowly decay and stabilized. Over time the graphs tend to nullify, which complies with δp^n states.

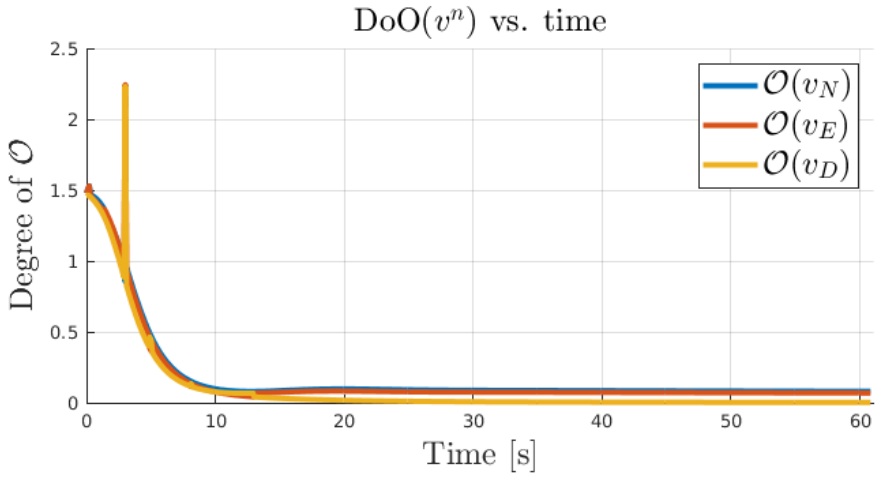

Here the velocity states DoO, exhibit an acute downhill and after approximately one second nullified. This can be explained by the position / velocity IMU coupling within the model.

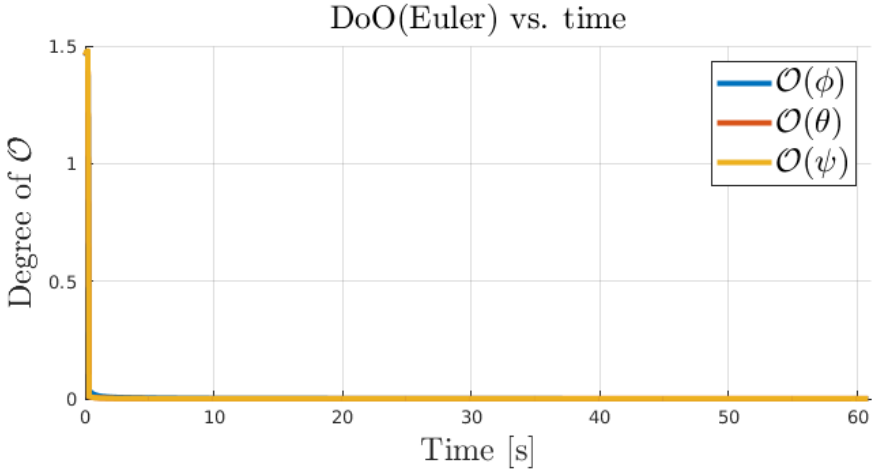

The vehicle is initialized stationary where noise measurements increase the residual measurement. But once motion is starting, the Euler angles' DoO immediately zero down after, implying that the estimator manages to succeed well in the estimating mission, although direct T_b^n measurement does not exist.

4.5 Partial estimation Performance

In order to examine the method's confidence when some states are missing, we changed the observation matrix H such that we don't get any latitude measurement information :

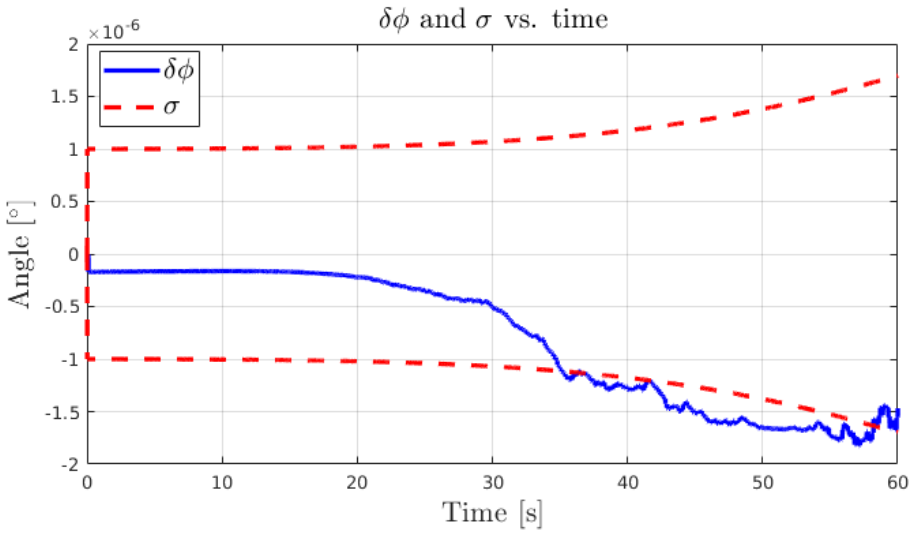

The angle error at a certain point out-bounds the σ (STD) graph and thus causes an acute drift. This is immediately being translated into high levels of DoO as can ben seen :

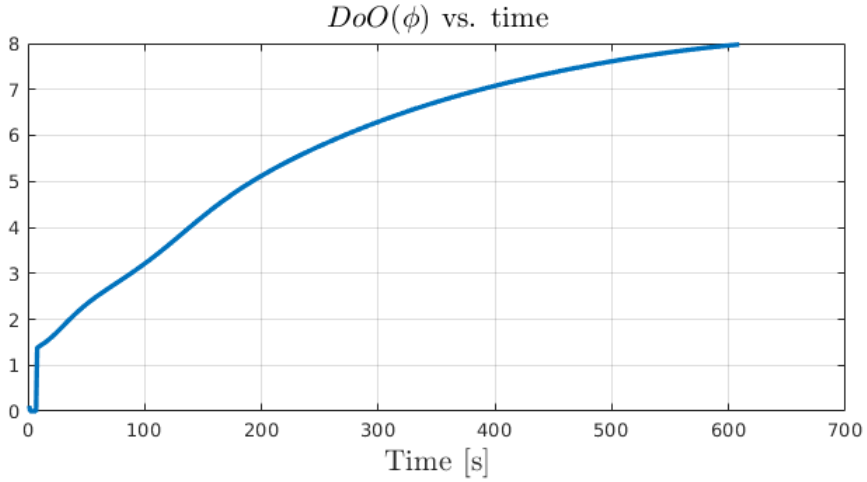

Which along time correspond to poor state estimation, and execution failure.

The final and most important expression of these deficient performance, can be seen in the overall trajectory, where the estimated course drifts badly w.r.t to the ground truth :

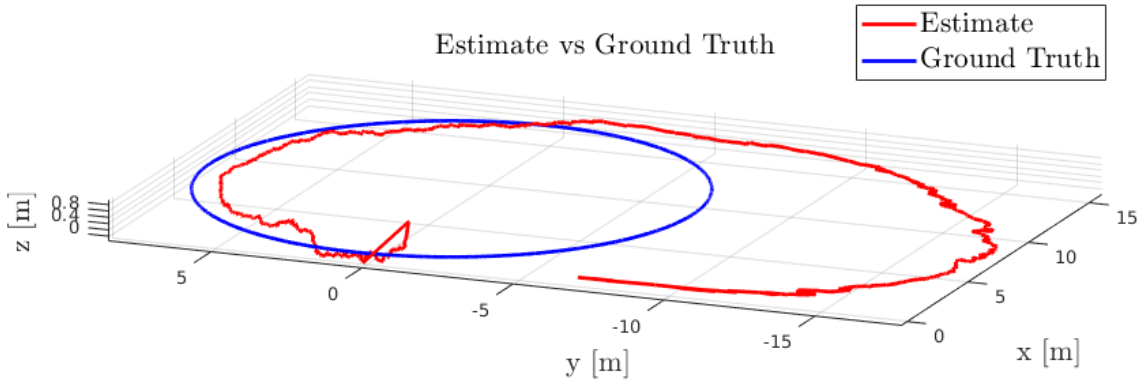

The observability graph can be seen thus, as an important sensor that measure quantitatively the estimation performances. Nonetheless, in the non-observability case, the degree figure shows us that there's indeed a growth in time, as expected. Hence, this method can be helpful in detecting a non-observable state.

4.6 Full estimation Performance

Finally, let us see the obtained trajectory under a full $\tilde{z}_{GPS}$ integration :

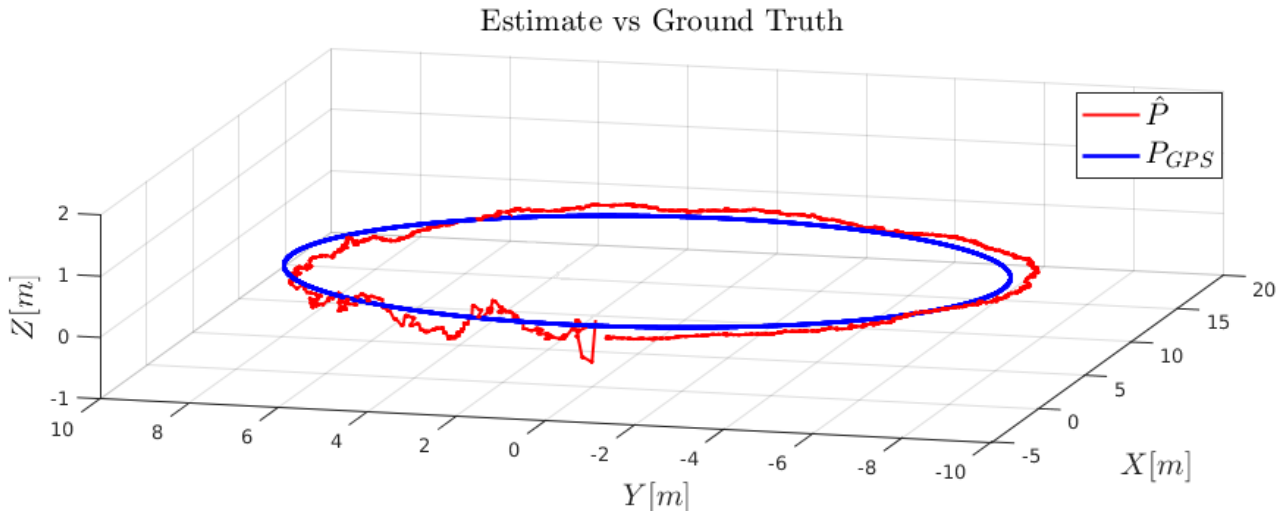

One can tell that the estimation mission succeeds impressively even under relatively large noise initialization. The estimated course keeps track with the ground truth under a fusion ration of 1:100. Navigating without any estimation would result as follows :

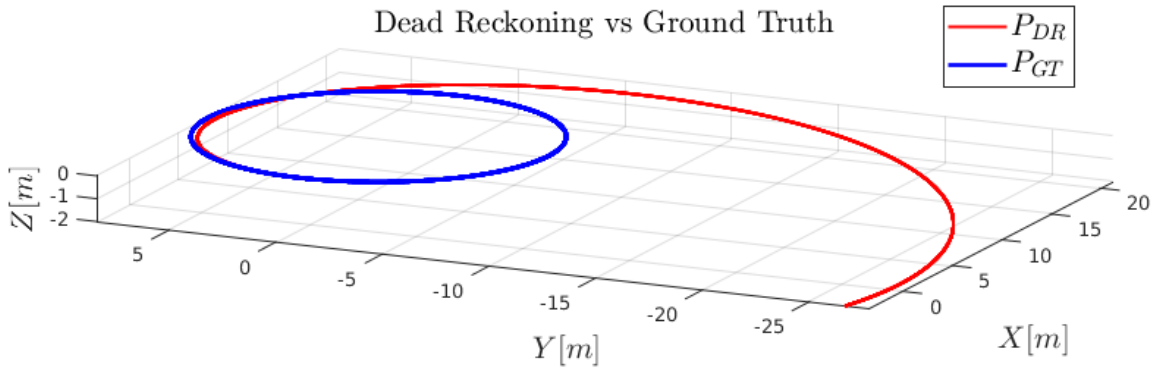

Needless to say that the noisy IMU overcomes within time, and the model drifts away uselessly. The last image shows the relation between measurement error and fusion ratio :

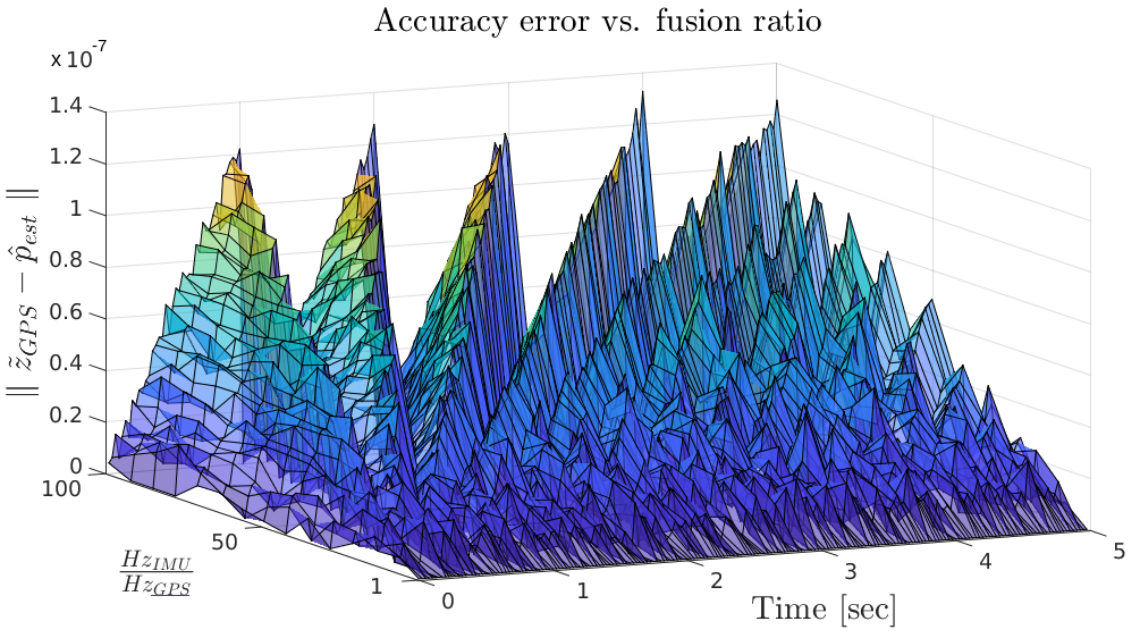

Based on the a varying set of fusion ratios (Eq. **3.6**), starting from 1:1 GPS correction follows every IMU prediction, up until seldom 1:100 ratio. Unsurprisingly, the more the GPS correction is frequent, the smaller the error is, and vice versa.

$-fin-$

5 Summary and Conclusions

• In this report, we implemented a full navigation solution with noised IMU and GPS sensors. The implementation consists of three main algorithms that we examined separately and together. The results show us that integrating the information from both sensors with Kalman Filter overcomes the disadvantages of using only one of the sensors at a time. On top of that, we investigated the various error trends w.r.t the STD calculated over time.

• We saw that the position and velocity errors converge to zero while the orientation errors remain small throughout the run. We assume the orientation doesn't converge to zero since there is an indirect connection between them and the GPS measurements. Another possible reason could be the error from the strapdown algorithm. Afterwards, we examined the filter with several different fusion ratios between GPS and IMU rates and saw that as the ratio gets higher the accuracy, but also the calculation's complexity grows.

• In addition, we have implemented a method for measuring the degree of observability of all states continuously. This measure has advantages over the classic observability measures. Firstly, it's continuous and by so can give us a qualitative information beyond yes / no answer and thus allows us to compare the 'degree' at different times of the run. Secondly, this measure is calculated with smaller complexity than the classic method.

• Other than that, we examined another case that did not appear in the original article, in which one state is not observable. This showed us that degrees of observability measure could be useful detecting a non-observable state in real time.

References

[1] Goshen-Meskin, D., and Bar-Itzhack, I.Y. (1992b) Observability analysis of piece-wise constant systems- Part II: Application to inertial navigation in-flight alignment. IEEE Transactions on Aerospace and Electronic Systems, 28, 4 (1992), 1068–1075.

[2] Wang, J., Lee, H.K., Hewitson, S., and Lee Hyung-Keun (2003). Influence of dynamics and trajectory on integrated GPS/INS navigation performance. Journal of Global Positioning Systems , 2 , 2 (2003) , 109-116.

[3] P. D. Groves, Principles of GNSS, inertial and multisensor integrated navigation systems, Artech House, 2013.

[4] J., A.Farrell, Aided navigation GPS with high rate sensors, McGraw-Hill, 2008.

[5] Shin E., N. El-sheimy, 2004. Report on the Innovate Calgary "Aided Inertial Navigation System (AINSTM) Toolbox", Calgary, Canada http://www.innovatecalgary.com/files/file/524-7-aided-inertial-navigation-system-ains-toolbox.pdf.

[6] Bar-Itzhack, I.Y., and Berman, N. (1988) Control theoretic approach to inertial navigation systems. Journal of Guidance, Control and Dynamics, 11, 3 (1988), 237- 245.

[7] Benson, D.O. (1975) A Comparison of two approaches to pure-inertial and doppler-inertial error analysis. IEEE Transactions on Aerospace and Electronic Systems, 11, 4 (1975), 447–455.

[8] Rhere, I., Abdel-Hafez, M., and Speyer, J. (2004) Observability of an integrated GPS/INS during maneuvers. IEEE Transactions on Aerospace and Electronic Systems, 40, 2 (2004), 526–535.

[9] . Ham, F., and Brown, R., Observability, eigenvalues, and Kalman filtering. IEEE Transactions on Aerospace and Electronic Systems, 19, 2 (1983), 269–273.

[10] Oliver J. Woodman (2007). "An introduction to inertial navigation", Cambridge CB3 0FD, IEEE Transactions on Aerospace and Electronic Systems. https://www.cl.cam.ac.uk/techreports/UCAM-CL-TR-696.pdf